

Dynamic graph based epidemiological model for COVID-19 contact tracing data analysis and optimal testing prescription

Shashanka Ubaru*

Lior Horesh

Guy Cohen

IBM T.J. Watson Research Center
Yorktown Heights, NY, USA

Abstract

In this study, we address three important challenges related to the COVID-19 pandemic, namely, (a) providing an early warning to likely exposed individuals, (b) identifying asymptomatic individuals, and (c) prescription of optimal testing when testing capacity is limited. First, we present a dynamic-graph based SEIR epidemiological model in order to describe the dynamics of the disease transmission. Our model considers a dynamic graph/network that accounts for the interactions between individuals over time, such as the ones obtained by manual or automated contact tracing, and uses a diffusion-reaction mechanism to describe the state dynamics. This dynamic graph model helps identify likely exposed/infected individuals to whom we can provide early warnings, even before they display any symptoms. When COVID-19 testing capacity is limited compared to the population size, reliable estimation of individual's health state and disease transmissibility using epidemiological models is extremely challenging. Thus, estimation of state uncertainty is paramount for both eminent risk assessment, as well as for closing the tracing-testing loop by optimal testing prescription. Therefore, we propose the use of arbitrary Polynomial Chaos Expansion, a popular technique used for uncertainty quantification, to represent the states, and quantify the uncertainties in the dynamic model. This design enables us to assign uncertainty of the state of each individual, and consequently optimize the testing as to reduce the overall uncertainty given a constrained testing budget. We present a few simulation results that illustrate the performance of the proposed framework.

1 Introduction

Contact tracing is considered one of the most effective methods to curb the spread of COVID-19 [8]. Contact tracing is a process by which the whereabouts and interactions of an infected individual with other individuals are carefully mapped. The key information that is sought is the physical proximity between individuals and for how long the individuals interacted. Additional information such as the environment where the interaction took place (for example, a close room with poor ventilation or an outdoor space) can also be recorded.

Contact tracing can be manual or digital. Manual contact tracing is usually performed by a contact tracer, a trained health-care worker, who interviews the infected individual. Based on the infected individual's recollection of events, calendar records, credit card records, etc. the contact tracer can build a list of exposed individuals that were in proximity to the infected individual and recommend action such as quarantine or testing of the exposed individuals. Digital contact tracing augments the work of a contact tracer. Individuals who participate in digital contact tracing typically carry a device that tracks their proximity to other individuals. As an example an individual's smart phone can be used to periodically transmit a unique identifier and also record transmissions of identifiers sent by nearby devices. The signal strength of the recorded transmissions can be used to estimate the proximity to other individuals [43, 11, 14, 34, 29, 3]. Digital contact tracing that relies on this method was recently implemented by Google and Apple [4] and is now available in most iOS and Android based smart phones. Digital contact tracing such as the one provided by Google and Apple is a crowd-sourcing method and its efficacy depends on adoption by the public. Furthermore, the method which uses Bluetooth transmission may inaccurately estimate of proximity due to signal

*Corresponding author, Shashanka.ubaru@ibm.com

attenuation or reflections from nearby objects. However, in the workplace, on university campuses, and in schools, contact tracing can be mandated. Active or passive devices like RFID bracelets or badges that are tracked by indoor sensors, can be used inside organization's campuses to obtain reliable and accurate digital contact tracing data. For the purpose of this work we assume that contact tracing data is obtained by any of the methods discussed above.

The recent COVID-19 pandemic has proved difficult to contain due to the large population of asymptomatic individuals. Asymptomatic people are individuals who are infected with the virus but have no symptoms. Asymptomatic people can be contagious to others. It is estimated that up to 40% of infected individuals are asymptomatic [25, 26, 45]. Identifying the asymptomatic individuals is therefore needed to successfully curb the spread of COVID-19. Testing for COVID-19 is another area that has proved to be difficult and has impeded the efforts to contain the virus. Without a doubt, testing is likely the most important tool that health-care professionals have to assess the spread of the virus within the population, yet the lack of testing kits and lab resources continues to limit testing volume. Additionally the cost of testing may also limit testing in disadvantaged communities. Since testing is a limited resource, testing the entire population periodically is not feasible and therefore it is of great importance to optimally prescribe testing.

Our contributions: In this paper we employ contact tracing data to infer which individuals are likely to be asymptomatic and which individuals should be tested to mitigate uncertainty of the overall network. We prescribe an optimal testing recommendations to mitigate the overall risk under the constraints of limited testing resources. To achieve these goals we start by representing the contact tracing data as a dynamic graph. Each node represents an individual, and connections between the nodes represents the interaction between individuals, such as physical proximity and duration of contact. We use a compartmental epidemiological model to evolve the graph in time. The evolution also incorporates new data from contact tracing as well as new testing data of individuals.

One of the epidemiological models that has been considered suitable for modeling COVID-19 is the SEIR model (Susceptible, Exposed, Infected, Recovered). This model takes into account an incubation period during which individuals that have been infected are not yet infectious themselves [22, 23, 24]. We note that our method is not tightly tied to the SEIR model and other models can be used if future studies suggest that other models better describe the spread of COVID-19. The SEIR model treats the entire population as a whole and is unaware of the connections and interaction between individuals. In this work we add graphical dependency to the SEIR model equations, so the details of how individuals interact impact the model accounting for the spread of the disease. The modified SEIR model is now described using a set of partial differential equations, with a graph Laplacian operator that accounts for the interaction between individuals as captured by the contact tracing data. In another deviation from the original SEIR model, we treat the S , E , I , R populations as probabilities [15], rather than compartmental populations.

Using the aforementioned model or a similar model, it is possible to provide an early warning to individuals who are likely to be exposed or infected and also identify those individuals who are likely to be asymptomatic. The latter have a high probability of being infected while showing no symptoms. The second challenge that we addressed is how to prescribe optimal testing while both targeting individuals conferring eminent risk to their surrounding as well as dedicating precious testing allocation towards providing a more accurate picture of the overall risk by mitigating the overall model uncertainty. Given the large-scale nature of the problem, we propose here a Polynomial Chaos Expansion (PCE) framework to offer a rapid means for sampling the posterior distribution of the state. Quantifiable assessment of the uncertainty associated with each node in the underlying state enables identification of nodes (e.g. nodes of high variance) in the graph in which point estimate predictions can provide spurious results. It is critical to judiciously assess the degree of confidence we can attribute to our predictions, and devise means to proactively mitigate uncertainty by testing, rather than merely settle with its quantification. For this, we propose optimal testing prescription by solving an optimization problem that accounts for (a) high risk individuals according to the model, (b) the uncertainty in the model, and (c) the testing budget available. We present simulation results that illustrate the models' behavior and show how we can issue early warnings to likely exposed/infected individuals and prescribe optimal testing to control uncertainty and mitigate the disease spread.

Related work: In the recent months, a plethora of works have been burgeoned in the literature that model the COVID-19 disease transmission. A number of variants of the SEIR model and other transmission models have been proposed, such as the SEIR models used to analysis the spread of COVID-19 in China [33, 41, 9, 26, 39], in Europe [15, 28, 27], in India [7, 36, 19] and in Africa [48]. Several other works exist too, that model the different aspects of

COVID [6, 18, 1, 20, 37] and others. However, to the best of our knowledge, our work is the first to incorporate contact tracing information into the SEIR model as dynamic graphs, with S, E, I, R populations as probabilities, to model the COVID-19 transmission. This enables us to issue early warnings to individuals who are likely to be exposed and/or infected. We also propose the use Polynomial Chaos Expansion to quantify uncertainties in the model and the measurements (test results) and present a method to prescribe optimal testing in order to control these uncertainties and mitigate the spread of the disease. These challenges have not been addressed in a systematic way in the prior works.

2 Problem formulation

For the sake of simplicity we assume a population of n individuals, yet, representation of varying population size over time can also be considered. We begin by defining notation of a probabilistic individualized pandemic state tensor, its dynamics and the measurement operations.

2.1 State

Let the state of the $i^{th} \in \mathbb{N}$ individual at time step $t \in \mathbb{N}$ be represented by the unit vector $y_{i,t} \in \mathbb{R}^4 = \{S_{i,t}, E_{i,t}, I_{i,t}, R_{i,t}\}$, where $y_{i,t}, S_{i,t}, E_{i,t}, I_{i,t}, R_{i,t} \in [0, 1]$ and the normalization condition applies $S_{i,t} + E_{i,t} + I_{i,t} + R_{i,t} = 1$. Thus, we assume that at each time step, an individual carries probabilities of being either susceptible, exposed, infected or recovered. The proposed framework is not restricted to the aforementioned choice, and obviously other probabilistic state representations corresponding to alternative pandemic models can equally be considered. Assuming T times steps has evolved from an initial state, the state of the dynamic system is represented by the 3^{rd} degree tensor $y \in \mathbb{R}^{n \times 4 \times T}$. Incorporation of a dynamic model (even mis-specified) offers means for the incorporation of a smooth temporal prior upon the evolution of these probabilities implicitly. The state can be enriched with stationary sites, such as public places, to enable transmission of disease via surface contact. Yet, proper representation of such sites may require a different state space representation as well as dedicated dynamics.

2.2 Measurements

2.2.1 Graph data

Let $G_t \in \mathbb{R}^{n \times n}$ represent weighed graph data attributed to each time step. The graph represents proximity interaction between individuals. The weights on the edges factors both proximity as well as exposure duration within a single time step. Such data can be acquired from peer-to-peer short-range communication on smart devices, such as Bluetooth [11, 5, 4, 3]. Since the interactions between individuals changes over time, the set of weighted graphs forms a dynamic graph over time. We shall denote the graph Laplacian of each temporal graph G_t , by $L_t \in \mathbb{R}^{n \times n}$.

2.2.2 Infection test data

In addition to the graph data, we shall assume that both IgM and IgG antigen may be administrated at each time step independently. IgM tests, qualify whether an individual is infected for the first time (attributed to the 3^{rd} components of individual's state at the timestep the test was collected). The number of IgM antigen tests taken at each time steps may vary and given by m_t , whereas the results of the tests are denoted by $d_t \in \mathbb{R}^{m_t}$, $m_t < n$. For the sake of data assimilation, we denote a linear projector operator $P_{d_t} \in \mathbb{R}^{m_t \times n}$ which projects the state at time step t to the IgM measurement space.

2.2.3 Recovery test data

Respectively, we shall denote by $p_t < n$ the number of IgG antigen tests taken at time step t and by $r_t \in \mathbb{R}^{p_t}$ the tests results. The IgG test qualifies whether an individual has been recovered. Similarly, as with the IgG tests, we define a linear projector $P_{r_t} \in \mathbb{R}^{p_t \times n}$ that projects the state at timestep t to the IgG measurement space.

2.2.4 Surface test data

Transmission of viral content can be made via stationary surfaces, rather than merely by face-to-face interaction of individuals [10, 35]. It is possible to incorporate into the pandemic transmission model tracing data representing interactions between individuals and physical sites (e.g. via interaction with stationary Bluetooth device or RF ID). Positive outcome of the test, will indicate that infectious particles were identified at a site. These tests can be treated similarly as IgM tests (attributed to the 3rd components of individual's state at the time step the test was collected) or otherwise can be handled differently by augmenting the SEIR model. The number of surface tests taken at each time steps is given by q_t , whereas the results of the tests are denoted by $s_t \in \mathbb{R}^{q_t}$, $q_t < n$. We denote a linear projector operator $P_{s_t} \in \mathbb{R}^{q_t \times n}$ which projects the state at time step t to the surface test space.

2.2.5 Cleaning / disinfecting event data

When physical sites are incorporated into the model, it is essential to indicate records of cleaning / disinfecting events which effectively reduce / reset the site to a state of having little probability of being infectious, that is annihilating the 3rd components of individual's state at the time step the test was collected. Let the number of such recorded events be denoted by $c_t < n$ with respective recorded values $v_t \in \mathbb{R}^{c_t}$. The linear projector $P_{v_t} \in \mathbb{R}^{c_t \times n}$ that projects the state at time step t to the disinfecting events.

2.3 Dynamics

To describe the dynamics of the model we modify the conventional SEIR population model, to an individualized, probabilistic graphical model. While the SEIR model has been employed extensively in disease control simulation, in the context of this study, other dynamical models can be equally utilized. Provided the interaction graph data between individuals over time as well as individuals pathogenic testing data, we shall recast the model as individualized model, where each node represents an individual, rather than address populations. Interactions between individuals and exchange of probabilities at the t^{th} timestep are represented using the graph Laplacian L_t . The revised model is a stochastic diffusion-reaction¹ model of the following form:

$$\frac{dS}{dt} = -\kappa_S L S - \beta E \odot S - \gamma I \odot S + \mu_s S \quad (1)$$

$$\frac{dE}{dt} = -\kappa_E L E + \beta E \odot S + \gamma I \odot S - \alpha E \quad (2)$$

$$\frac{dI}{dt} = -\kappa_I L I + \alpha E - \mu_h I - \mu_s S \quad (3)$$

$$\frac{dR}{dt} = \mu_h I \quad (4)$$

where $\kappa_S, \kappa_E, \kappa_I \in \mathbb{R}$ are diffusion coefficients and $\alpha, \beta, \gamma, \mu_h, \mu_s \in \mathbb{R}$ represent reaction coefficients. The model coefficients can be prescribed a-priori, but, whenever sufficient data is provided, these coefficients can be learned statistically². The coefficients of the model themselves may evolve over time to reflect changes in individuals behaviour (e.g. masks wearing compliance, hand sanitation frequency, etc). Such refinements of the model can be accommodated by devising parametric / non-parametric models for the coefficients themselves, that includes additional health-care policies and public compliance affinity parameters. Furthermore, structural mis-specification of the dynamical model can be mitigated via hybridization of first-principle and data-driven model learning [40, 38]. Other than advocating for models that enables probabilistic treatment of individual state, and the incorporation of graphical data, the scope of this study focuses on closure of the tracing-sensing loop, rather than the intricacies of any particular model. Thus, for the sake of expositional simplicity we shall proceed with the above exemplar model.

Integration of the aforementioned continuous-time dynamical system (1) can be performed in various ways, such as implicit-explicit combination, high order Runge-Kutta integrators, etc. Given the frequent rate of the graph data,

¹It is important to note that other than the diffusion-reaction model considered here, alternate transport models such as wave relaxation, etc, can be considered. The discussion of such models goes beyond the scope of this study

² Diffusion and reaction coefficients may be set a-priori differently to model individuals dynamics, vs. sites.

and the complexity associated with semi-explicit integration schemes, we shall resort here to a simple forward Euler integration. Obviously, when such explicit integrator is employed it is essential to ensure stability of the numerical solution via careful selection of timestep duration. Other, more complex integration schemes can equally be considered. Under these settings we have:

$$S_{t+1} = S_t - \Delta t(\kappa_S L_t S_t + \beta E_t \odot S_t + \gamma I_t \odot S_t) \quad (5)$$

$$E_{t+1} = E_t - \Delta t(\kappa_E L_t E_t - \beta E_t \odot S_t - \gamma I_t \odot S_t + \alpha E_t) \quad (6)$$

$$I_{t+1} = I_t - \Delta t(\kappa_I L_t I_t - \alpha E_t + \mu I_t) \quad (7)$$

$$R_{t+1} = R_t + \Delta t \mu I_t \quad (8)$$

The initial conditions of the model are generally unknown a-priori. In the following section, we shall discuss how uncertainty associated with these conditions can be quantified and mitigated.

Data Assimilation In order to provide point estimate of the state y given measurements (testing) up till $t = T$, we can consider a dynamic inverse problem that accounts the IgM and IgG antigen tests and the associated noise in the models. Such a point estimator can be useful, yet they do not provide means for estimation of the posterior probability, and therefore, can be limiting when it comes to uncertainty quantification, and experimental design. Conventionally, one can sample the prior distribution associated with the state and update the posterior using methods such as Markov Chain Monte (MCMC) Carlo or Hamiltonian Monte Carlo. Alternatively, methods such as generalized and arbitrary Polynomial Chaos Expansions can offer more salable means to sample the posterior in large-scale settings [13, 31, 2].

3 Uncertainty Control

Due to limited testing capacity, in most cases testing is performed sparsely, where the number of tests is significantly smaller compared to the dimensions of the state space $\sum_{t=t_0}^T m_t < \sum_{t=t_0}^T n$, rendering the state inference problem to be ill-posed. Furthermore, the intrinsic recovery function, the interaction dynamics, and the measurements are all mis-specified, and therefore admitting uncertainty. Assuming some form of regularity of the solution (primarily in the form of the dynamical model), we can still make substantiated inferences, yet, we must consciously account for the underlying uncertainty associated with each inference. Whenever an observation (testing) takes place, one can attribute relatively high degree of confidence (small uncertainty) to the probability assigned to the relevant node, yet, the further we move away from that node across the graph, or propagate over time, the level of confidence decays.

Appropriate representation of uncertainty, is critical for making judicious decision as for how to prioritize best the administration of a limited testing budget. This overarching mission is essence of this study. On the one hand, it is eminent to test those identified to be under high risk (high probability of being infected), as such individuals confer immediate risk to their surrounding, yet on the other hand, acknowledging the limitation of the model, we wish to allocate testing as to reduce the degree of uncertainty associated with nodes for which uncertainty is high, as we otherwise, favor exploitation over exploration, and may miss the bigger picture altogether.

3.1 Polynomial Chaos Expansion

Polynomial Chaos Expansion (PCE) is a popular tool used for the quantification of prediction uncertainties in stochastic systems [16, 47, 31]. The idea is to reduce the model that are computationally expensive to simulate, into a parametric form by representing the model in terms of a basis of orthonormal polynomials with respect to the input random variables. PCE has recently been used for modeling systems in a number of applications, including machine learning [42], sensitivity analysis of systems [12], flow simulations [47], geo-spatial statistics [32, 30], integrated circuits [21] and others. Different variants of PCE have been proposed, where the methods differ with respect to the polynomial considered [46, 47, 31], and the approaches used for computing the coefficients [16, 13].

In this paper, we consider the arbitrary Polynomial Chaos Expansion (aPCE) approach proposed in [31], which is a data driven approach for analyzing the stochastic (dynamical) system. In particular, we consider the Bayesian variant of aPCE [30]. The method only requires knowledge of the moments of the input random variable, and does not require its probability distribution. Consider a stochastic system $y(\xi)$ with multi-dimensional input random variable $\xi = \{\xi_1, \dots, \xi_N\}$. In our case, we can consider the state S, E, I, R as four different stochastic PDE models, and the N parameters to be the state of the N -nearest neighbours in the graph. We wish to represent $y(\xi)$ by a multivariate polynomial expansion as follows:

$$y(\xi) \approx \sum_{i=1}^M c_i \Phi_i(\xi), \quad (9)$$

where the coefficients c_i are quantify the dependence of the y on the input parameters ξ . The number of terms in the expansion M is given as $M = \frac{(N+d)!}{N!d!}$, where n is the number of parameters and d is the expansion order. Φ_i 's are the multi-variate orthogonal polynomial basis for $\{\xi_1, \dots, \xi_N\}$, and assuming the parameters to be independent, we express

$$\Phi_i(\xi) = \prod_{j=1}^N P_j^{(\theta_j^i)}(\xi),$$

with $\sum_j \theta_j^i \leq M$ (multivariate indices that contains the combinatoric information). In the moment based PCE methods, the polynomials are defined as:

$$P^{(k)}(\xi) = \sum_{l=1}^k \rho_l^{(k)} \xi^l, \quad l \in [0, d],$$

where $\rho_l^{(k)}$ are coefficients of $P^{(k)}$.

The method in [31, 30] constructs these polynomials for any arbitrary distributions using the just moments computed from observed/sampled data. The polynomials are computed by solving a linear system with a particular square matrix of moments, see [31] for details. The coefficients are computed using GramSchmidt orthogonalization or by the Stieltjes procedure based on the observed data. The coefficients can be then updated using a Bayesian approach for the additional observed/sample data, see [30].

In our case, the measurements correspond to the testing results d_t and r_t . Once, we obtain the PCE, we can compute the posterior statistics such as posterior mean $\hat{\mu}$ and variance $\hat{\sigma}$ for the output model, inexpensively simply constructing the response surface using the coefficients of the polynomial expansion. In our case, we can obtain the posterior mean and variance for the four states for each individual using aPCE. The posterior statistics can then be used to identify uncertainties in the individual's states, and optimal testing can be prescribed.

3.2 Optimal testing prescription

One of the main challenges related to the COVID-19 pandemic has been the issue of prescribing testing optimally given limited testing resources. The aPCE approach described above helps us quantify uncertainty, and using the posterior statistics, we can prescribe optimal testing to control/mitigate the uncertainty.

Suppose the probability associated with each state y_t be denoted by a 2^{nd} moment construct accounting for both the mean probability μ_t and the variance σ_t , representing the state uncertainty, i.e. $y_t \sim \mathcal{N}\{\mu_t, \sigma_t I\}$. Our goal would be to figure out what is the best testing paradigm in the next time step, so as to (a) minimize the risk of infection propagation, while also (b) minimize the uncertainty associated with the state, and (c) account for the limited testing budget. Let, $w_t \in \mathbb{R}_+^n$ denote the recommended testing assignment for the time step t . Then, we propose to solve the following problem:

$$\hat{w}_t = \arg \min_{w_t} \{U(w_t, \hat{\sigma}_t) + D(w_t, a(\hat{\mu}_t, \hat{\sigma}_t), d_t) + \lambda \|w_t\|_1\} \quad (10)$$

$$\text{s.t.} \quad 0 \leq w_t \leq 1 \quad (11)$$

where function $U(\cdot)$ represents the posterior uncertainty (measured using the posterior of variance $\hat{\sigma}_t$ computed using PCE) associated with performing tests per d_t , and function $D(\cdot)$ captures the degree in which testing should be performed to those who are in the highest risk of being infected (a form of bias-variance balance), with $a(\cdot)$ is a distance

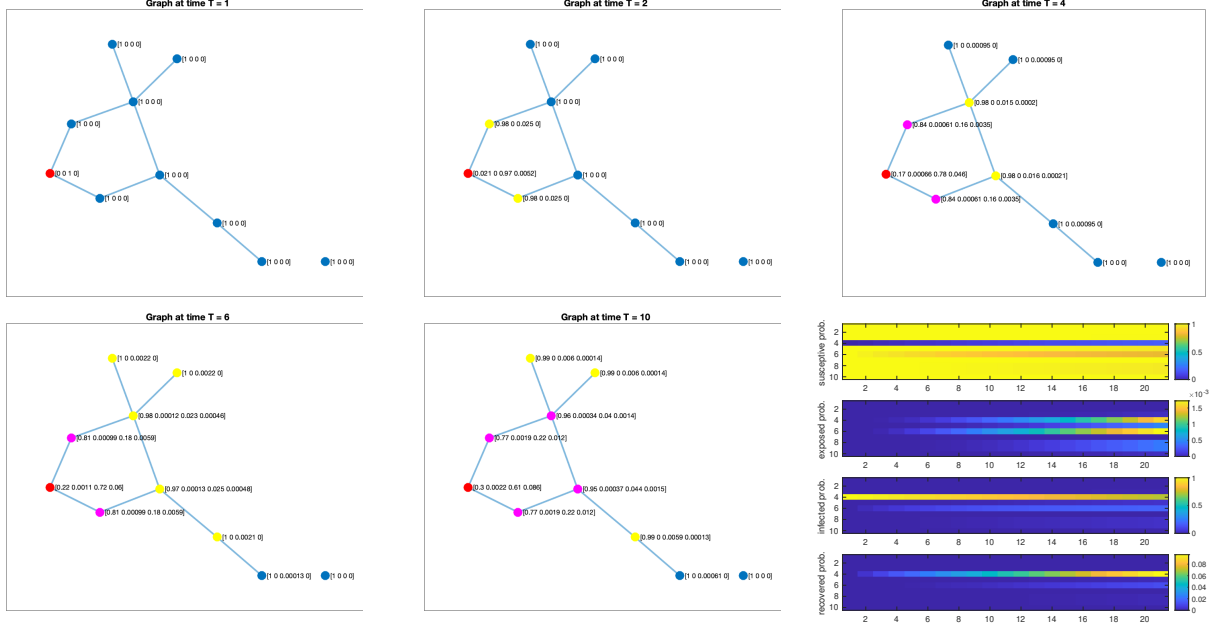


Figure 1: Graphical SEIR model disease transmission visualization. Sample simulation with 10 nodes at five time instances (first five images). Red nodes indicate infected individuals $I > 0.5$, magenta nodes have $I > 0.04$, and yellow have $I > 0.002$. The last plot depicts the state $\{S, E, I, R\}$ for the 10 individuals over 20 time instances.

measure that quantify the discrepancy between infected symptomatic and asymptomatic individual. The ℓ_1 regularization is used to control the sparsity of w_t , i.e, the number of tests to be performed at time t , based on the testing budget available. ℓ_0 norm cardinality constraint (non-convex) can also be used for a fixed test budget, say $\|w_t\|_0 \leq k_t$, where k_t is the maximum number of tests available at time t [44]. We can also split the problem into two separate minimization problems in order to assign predefined budget to the two criteria (risk and uncertainty).

4 Simulation Results

In this section, we present few numerical results based on simulations to illustrate the behaviour of the different aspects of our models. We first show how the graphical SEIR model captures the disease dynamics, and how we can use it to issue early earnings to individuals who are likely infected/exposed. We then show how aPCE and uncertainty quantification can be used to prescribe optimal testing, when the testing resources are limited.

Graphical SEIR model: In the first set of experiments, we analyze the graphical SEIR model proposed in section 2. In figure 1, we illustrate the disease transmission as modelled by the graphical SEIR model. We consider a small (fixed) graph of 10 individuals (for easy visualization) and show how the infection transmits to other nodes over time. At time step $t = 1$, we have one individual infected (red node). We note that as time evolves, the infection spreads to nodes who are at close proximity. We consider a fixed graph here for illustration, but a graph that varies over time (better simulation of human interactions) is considered in the remaining experiments. We note that the state of the nodes evolve over time as the virus spreads. As examples, we have magenta nodes with $I > 0.04$, and the yellow nodes with $I > 0.002$, and we note the change of states over time. Based on this model, we can *issue early warnings* to the individuals (via. text messages or app notifications) if their state I or E crosses certain thresholds, possibly even before the individuals show any symptoms. In our example, we can send out warnings to the individuals, when their colors change, once when blue to yellow and again when yellow to magenta.

The last plot depicts the state $\{S, E, I, R\}$ for the 10 individuals over 20 time instances. We note that the

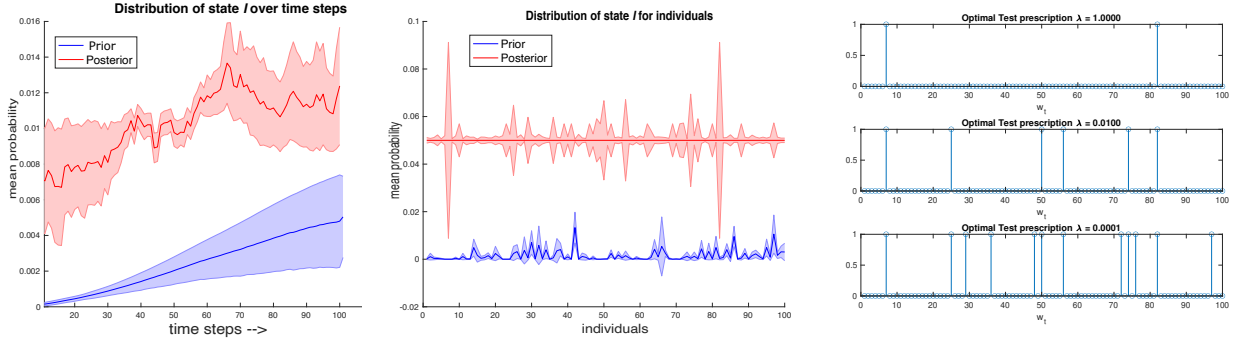


Figure 2: PCE and Optimal testing: (Left) Prior and Posterior distributions [mean with standard deviation error band] of the infection state over time steps t . (Middle) Prior and Posterior distributions of the infection state for 100 individuals. (Right)- The optimal testing prescription vector w_t for different values of regularization parameter $\lambda \in [1, 0.01, 0.0001]$.

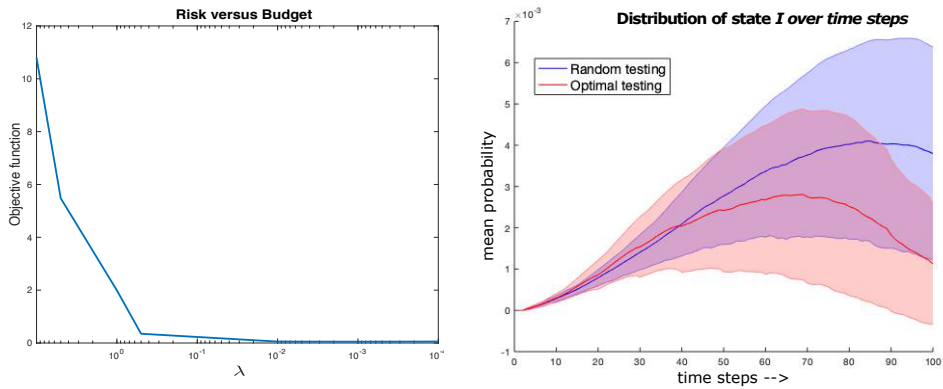


Figure 3: PCE and Optimal testing: (Left) Trade-off between the risk (objective function in (10)) versus the testing budget (regularization parameter λ i.e., no. of tests), and (Right) Distribution [mean with standard deviation error band] of state I over time with random and optimal testing.

model accounts for both spread of the virus, as well as how the infected individuals recover (and possibly become susceptible again). The rate of change of the states can be optimized by tuning the different parameters (the diffusion coefficients $\kappa_S, \kappa_E, \kappa_I$ and the reaction coefficients $\alpha, \beta, \gamma, \mu_h, \mu_s$) in the model based on data observations, geographical locations, and time. In our experiments, we chose $\kappa_S = 0.1, \kappa_E = 0.1, \kappa_I = 0.25$, and $\alpha = 0.02, \beta = 0.05, \gamma = 0.01, \mu_h = \mu_s = 0.05$. The statistical distributions for individuals and over time steps are discussed in the next results (see Prior distributions in Figure 2). All simulations were performed on Matlab, and our code will be made publicly available.

PCE and optimal testing: In the next set of experiments, we study the different aspects of the PCE analysis and uncertainty control. We summarize these results in Figure 2 and 3. The first (left) plot in Figure 2 gives the prior and posterior distributions in the form of the mean with the standard deviation error band of the infection state I over time steps. We considered $n = 1000$ individuals to compute the statistics and total time steps $T = 100$. The prior distribution is the distribution of the state over time steps as obtained (evolved) from our graphical SEIR model. The posterior distribution is obtained by representing the state using Bayesian aPCE [30] and computing the response surface using the measurements (uniformly random testing results). We built our PCE simulation using the source code made available by the authors of [30]. For PCE, we chose no. of input parameters $N = 5$, i.e., we consider N nearest neighbours (based on the edge weights), and the expansion order $d = 3$. Hence, the no. of terms (Collocation Points) was $M = 56$ (same parameters were used in all experiments). We observe that the prior distribution is smooth and increasing. This is because the SEIR model does not account for testing. The posterior distribution is random, due to the random testing measurements.

In the second (middle) plot, we give the prior and posterior distributions for each individuals obtained from the PCE analysis. We plot the statistics for 100 individuals (we chose fewer nodes for easy visualization) computed over 100 time instances. Again, the posterior distribution is estimated using the response surface computed using Bayesian aPCE with the above parameters. We observe that the state of certain individuals have high variance (high uncertainty). In the last (right) plot, we display the optimal testing prescription vector w_t (rounded to $\{0, 1\}$) we obtained by solving the optimization in (10) for different regularization parameter $\lambda \in [1, 0.01, 0.0001]$. Simple ℓ_2 norm functions were used for both $U(\cdot)$ and $D(\cdot)$ functions, and the Matlab CVX package [17] was used to solve the optimization problem. We first observe that, as we decrease λ , the cardinality of w_t , i.e., the no. of prescribed tests increases. We can choose an optimal λ value based on the available budget. Moreover, we observe that the method prescribes testing for individuals with high uncertainty. Note that as no. of prescribed tests is increased, more individuals with high variance in middle plot are prescribed. These results show that we can quantify the uncertainty in our model and prescribe appropriate testing.

In Figure 3 we further analyze the optimal testing prescription. The left plot in the figure presents the *risk to budget trade-off* by plotting the final value of objective function in (10) we obtained for the optimal w_t for different values of the regularization parameter λ . We again chose $n = 1000$, $T = 100$, and other parameters as before. Decreasing λ increases the no. of prescribed tests, and in turn the testing budget required. The plot shows that increasing the no. of tests reduces the risk initially and after a point this reduction is minimal. The trade-off plot helps us to choose an optimal λ (lowest testing budget) for an acceptable risk tolerance.

The right plot in the Figure 3, presents the distribution of the infection state I over time steps t when testing was conducted randomly (in blue) and when optimal testing was prescribed at regular intervals (in red). We considered $T = 100$ time steps, and in the first case, we performed random testing at each time instance. In the second case, we ran the PCE analysis after every 10 time instances (use previous 10 random measurements to construct the PCE) and used the optimal testing prescription in the next instance. We observe that in the second case, the mean infection starts reducing sooner than the random testing. These results suggest that indeed prescribing optimal testing can help control uncertainty and mitigate disease transmission.

Conclusions

In this study, we introduced a probabilistic SEIR model for COVID-19 transmission. The model represents individual-level contact tracing information via dynamic graphs, where each individual represent a node and interaction is described by edges. The S , E , I , R compartments are treated as probabilistic entities as to capture uncertainty associated with the stochastic process of disease propagation, sparse COVID-19 testing, and model inadequacies. As illustrated by numerical simulations, this model can help healthcare professionals in issuance of early warnings to individuals who are likely exposed or infected by COVID-19. Furthermore, the model identifies those individuals who are likely to be asymptomatic. We then proposed the use of arbitrary Polynomial Chaos Expansion (aPCE) to quantify uncertainties in the model, while maintaining computational scalability. By estimating the expected risk as well as minimizing uncertainty we prescribe optimal testing for individuals under limited testing and tracing resources. The framework offers a decision tool for balancing between immediate disease spread threat intervention and informed assessment of the pandemic state. Lastly, the framework provides means for policy makers as to estimate the required testing budget for a given acceptable risk tolerance.

References

- [1] D. Acemoglu, V. Chernozhukov, I. Werning, and M. D. Whinston. A multi-risk sir model with optimally targeted lockdown. Technical report, National Bureau of Economic Research, 2020.
- [2] R. Ahlfeld, B. Belkouchi, and F. Montomoli. Samba: sparse approximation of moment-based arbitrary polynomial chaos. *Journal of Computational Physics*, 320:1–16, 2016.
- [3] H. Alsdurf, Y. Bengio, T. Deleu, P. Gupta, D. Ippolito, R. Janda, M. Jarvie, T. Kolody, S. Krastev, T. Maharaj, et al. Covi white paper. *arXiv preprint arXiv:2005.08502*, 2020.

- [4] Apple-Google. Apple-google exposure notification. <https://www.google.com/covid19/exposurenotifications/>, <https://www.apple.com/covid19/contacttracing/>, 2020.
- [5] Y. Bengio, R. Janda, Y. W. Yu, D. Ippolito, M. Jarvie, D. Pilat, B. Struck, S. Krastev, and A. Sharma. The need for privacy with public digital contact tracing during the covid-19 pandemic. *The Lancet Digital Health*, 2020.
- [6] D. W. Berger, K. F. Herkenhoff, and S. Mongey. An seir infectious disease model with testing and conditional quarantine. Technical report, National Bureau of Economic Research, 2020.
- [7] K. Biswas and P. Sen. Space-time dependence of corona virus (covid-19) outbreak. *arXiv preprint arXiv:2003.03149*, 2020.
- [8] CDC. Cdc coronavirus disease 2019 (covid-19). <https://www.cdc.gov/coronavirus/2019-ncov/php/open-america/contact-tracing-resources.html>, 2020.
- [9] Y.-C. Chen, P.-E. Lu, C.-S. Chang, and T.-H. Liu. A time-dependent sir model for covid-19 with undetectable infected persons. *arXiv preprint arXiv:2003.00122*, 2020.
- [10] L. Cirrincione, F. Plescia, C. Ledda, V. Rapisarda, D. Martorana, R. E. Moldovan, K. Theodoridou, and E. Cannizzaro. Covid-19 pandemic: Prevention and protection measures to be adopted at the workplace. *Sustainability*, 12(9):3603, 2020.
- [11] G. Cohen and L. Horesh. Crowd sourced contact tracing, informing and prevention of virus contagion with privacy preservation, 2020.
- [12] T. Crestaux, O. Le Maitre, and J.-M. Martinez. Polynomial chaos expansion for sensitivity analysis. *Reliability Engineering & System Safety*, 94(7):1161–1172, 2009.
- [13] B. J. Debusschere, H. N. Najm, P. P. Pēbay, O. M. Knio, R. G. Ghanem, and O. P. Le Maitre. Numerical challenges in the use of polynomial chaos representations for stochastic processes. *SIAM journal on scientific computing*, 26(2):698–719, 2004.
- [14] DP3T. Dp3t - decentralized privacy-preserving proximity tracing. <https://github.com/DP-3T/documents>, 2020.
- [15] D. Faranda and T. Alberti. Modelling the second wave of covid-19 infections in france and italy via a stochastic seir model. *arXiv preprint arXiv:2006.05081*, 2020.
- [16] R. G. Ghanem and P. D. Spanos. *Stochastic finite elements: a spectral approach*. Courier Corporation, 2003.
- [17] M. Grant and S. Boyd. *Cvx: Matlab software for disciplined convex programming*, 2009.
- [18] V. Guerrieri, G. Lorenzoni, L. Straub, and I. Werning. Macroeconomic implications of covid-19: Can negative supply shocks cause demand shortages? Technical report, National Bureau of Economic Research, 2020.
- [19] R. Gupta and S. K. Pal. Trend analysis and forecasting of covid-19 outbreak in india. *medRxiv*, 2020.
- [20] C. J. Jones, T. Philippon, and V. Venkateswaran. Optimal mitigation policies in a pandemic: Social distancing and working from home. Technical report, National Bureau of Economic Research, 2020.
- [21] A. Kaintura, T. Dhaene, and D. Spina. Review of polynomial chaos-based methods for uncertainty quantification in modern integrated circuits. *Electronics*, 7(3):30, 2018.
- [22] W. Kermack and A. McKendrick. Contributions to the mathematical theory of epidemics i. *Bulletin of Mathematical Biology*, 53(1-2):3355, 1991.
- [23] W. Kermack and A. McKendrick. Contributions to the mathematical theory of epidemics ii. the problem of endemicity. *Bulletin of Mathematical Biology*, 53(1-2):5787, 1991.

- [24] W. Kermack and A. McKendrick. Contributions to the mathematical theory of epidemics iii. further studies of the problem of endemicity. *Bulletin of Mathematical Biology*, 53(1-2):89118, 1991.
- [25] R. Li, S. Pei, B. Chen, Y. Song, T. Zhang, W. Yang, and J. Shaman. Substantial undocumented infection facilitates the rapid dissemination of novel coronavirus (sars-cov-2). *Science*, 368(6490):489–493, 2020.
- [26] J. Liu, L. Wang, Q. Zhang, and S. T. Yau. The dynamical model for covid-19 with asymptotic analysis and numerical implementations. *Applied Mathematical Modelling*, 2020.
- [27] L. López and X. Rodó. The end of social confinement and covid-19 re-emergence risk. *Nature Human Behaviour*, 4(7):746–755, 2020.
- [28] L. López and X. Rodo. A modified seir model to predict the covid-19 outbreak in spain and italy: simulating control scenarios and multi-scale epidemics. *Available at SSRN 3576802*, 2020.
- [29] NHS. NHS covid-19 app. <https://www.nhsx.nhs.uk/covid-19-response/nhs-covid-19-app/>, 2020.
- [30] S. Oladyshkin, H. Class, and W. Nowak. Bayesian updating via bootstrap filtering combined with data-driven polynomial chaos expansions: Methodology and application to history matching for carbon dioxide storage in geological formations. *Computational Geosciences*, 08 2013.
- [31] S. Oladyshkin and W. Nowak. Data-driven uncertainty quantification using the arbitrary polynomial chaos expansion. *Reliability Engineering & System Safety*, 106:179–190, 2012.
- [32] S. Oladyshkin, P. Schröder, H. Class, and W. Nowak. Chaos expansion based bootstrap filter to calibrate co2 injection models. *Energy Procedia*, 40:398–407, 2013.
- [33] L. Peng, W. Yang, D. Zhang, C. Zhuge, and L. Hong. Epidemic analysis of covid-19 in china by dynamical modeling. *arXiv preprint arXiv:2002.06563*, 2020.
- [34] PEPP. Pan-european privacy-preserving proximity tracing. <https://pepp-pt.org/>, 2020.
- [35] D. Pradhan, P. Biswasroy, G. Ghosh, G. Rath, et al. A review of current interventions for covid-19 prevention. *Archives of medical research*, 2020.
- [36] T. Sardar, S. S. Nadim, and J. Chattopadhyay. Assessment of 21 days lockdown effect in some states and overall india: a predictive mathematical study on covid-19 outbreak. *arXiv preprint arXiv:2004.03487*, 2020.
- [37] I. B. Schwartz, J. H. Kaufman, K. Hu, and S. Bianco. Predicting the impact of asymptomatic transmission, non-pharmaceutical intervention and testing on the spread of covid19. *medRxiv*, 2020.
- [38] G. Shulkind, L. Horesh, and H. Avron. Experimental design for nonparametric correction of misspecified dynamical models. *SIAM/ASA Journal on Uncertainty Quantification*, 6(2):880–906, 2018.
- [39] P. X. Song, L. Wang, Y. Zhou, J. He, B. Zhu, F. Wang, L. Tang, and M. Eisenberg. An epidemiological forecast model and software assessing interventions on covid-19 epidemic in china. *MedRxiv*, 2020.
- [40] J. T. Thorson, K. Ono, and S. B. Munch. A bayesian approach to identifying and compensating for model misspecification in population models. *Ecology*, 95(2):329–341, 2014.
- [41] C. Tian, Q. Zhang, and L. Zhang. Global stability in a networked sir epidemic model. *Applied Mathematics Letters*, page 106444, 2020.
- [42] E. Torre, S. Marelli, P. Embrechts, and B. Sudret. Data-driven polynomial chaos expansion for machine learning regression. *Journal of Computational Physics*, 388:601–623, 2019.
- [43] TraceTogether. Singapore tracetogether app. <https://www.tracetogether.gov.sg/>, 2020.

- [44] E. Van Den Berg and M. P. Friedlander. Probing the pareto frontier for basis pursuit solutions. *SIAM Journal on Scientific Computing*, 31(2):890–912, 2009.
- [45] S. J. Weinstein, M. S. Holland, K. E. Rogers, and N. S. Barlow. Analytic solution of the seir epidemic model via asymptotic approximant. *Physica D: Nonlinear Phenomena*, 411:132633, 2020.
- [46] D. Xiu and G. E. Karniadakis. The wiener–askey polynomial chaos for stochastic differential equations. *SIAM journal on scientific computing*, 24(2):619–644, 2002.
- [47] D. Xiu and G. E. Karniadakis. Modeling uncertainty in flow simulations via generalized polynomial chaos. *Journal of computational physics*, 187(1):137–167, 2003.
- [48] Z. Zhao, X. Li, F. Liu, G. Zhu, C. Ma, and L. Wang. Prediction of the covid-19 spread in african countries and implications for prevention and controls: A case study in south africa, egypt, algeria, nigeria, senegal and kenya. *Science of the Total Environment*, page 138959, 2020.